



Measurement of Size Resolved Burning of Metal Nanoparticles for Evaluation of Combustion Mechanisms

Rohit J. Jacob¹, Yichen Zong², Yong Yang³
Department of Chemical and Biomolecular Engineering
University of Maryland, College Park, Maryland, 20742, USA

Shuiqing Li⁴
Key laboratory for Thermal Science and Power Engineering of Ministry of Education
Department of Thermal Engineering, Tsinghua University, Beijing, 100084, China

and

Michael R. Zachariah⁵
Department of Chemical and Biomolecular Engineering
University of Maryland, College Park, Maryland, 20742, USA

While metal nanoparticles are of interest as high energy density additives there is still considerable uncertainty on the combustion mechanism and the size dependent burning exponent. In this work, we probe the oxidation kinetics of metal nanoparticles by evaluating their size dependent burn rate. In particular, to answer why many measurements in the literature indicate a low fraction power dependence to the burning rate. Nanoparticles of titanium and zirconium in the size range of 20-150 nm were produced by pulsed laser ablation of a metal target, and electrostatically size selected using a differential mobility analyzer (DMA). The highly dilute aerosol of the size-selected metal particles were subsequently injected into a high temperature (1700 – 2500K), oxidizing zone produced by the post flame region of a laminar diffusion flame. The emission profiles of the particle combustion were monitored using high speed videography from which burn rate measurements were made. Particle burn time scaling laws of the form $t = a(\text{diameter})^b$ are established which highlights the significance of sintering of the nanoparticle aggregates prior to significant reaction. Our results indicate that once sintering is accounted for, the rate of combustion follows a near (diameter)¹ power-law dependence. Additionally, Arrhenius parameters for the combustion of these nanoparticles were also evaluated. The emission traces from particle combustion was fit to existing models of solid state oxidation so as to extract mechanistic information about the underlying process, which we find can be reasonably described with a kinetically controlled shrinking core model. The results indicate that sintering is rapid for nanostructures, which impacts the burning rate negatively. A few comments on a possible strategy to maximize the potential of nanoenergetics by suppressing rapid, pre-reaction sintering is proposed.

¹ Graduate Research Assistant, Department of Chemical and Biomolecular Engineering.

² Visiting student, Department of Chemical and Biomolecular Engineering.

³ Graduate Research Assistant, Department of Chemical and Biomolecular Engineering.

⁴ Professor, Department of Thermal Engineering, Tsinghua University.

⁵ Professor, Department of Chemical and Biomolecular Engineering (mrz@umd.edu).

Nomenclature

Z_P	=	Particle mobility
Q_{sh}	=	DMA sheath flow rate
V	=	applied voltage
L	=	length of the DMA
R_2	=	Outer diameter of the DMA
R_1	=	Inner diameter of the DMA
e	=	Total charge on particle
C	=	Cunningham Slip correction
d_m	=	Mobility equivalent spherical diameter
μ	=	gas viscosity
d_p	=	Primary particle size
N	=	Number of particles in an aggregate
D^*	=	Estimated particle size after sintering (based on volume conservation)
α	=	Conversion factor
X_{Ti}	=	Volume fraction of Titanium/ Zirconium core left
τ	=	Burn time [s]
T	=	Particle Temperature [K]
m_g	=	Air molecular weight ($4.8 \cdot 10^{-26}$ Kg)
K	=	Boltzmann Constant ($1.38 \cdot 10^{-23}$ m ² Kg s ⁻² K ⁻¹)
P_g	=	Gas Pressure (1 atm)
γ	=	Adiabatic expansion factor (=1.3 at 1500 K)
T_g	=	Gas Temperature (1750 K)
σ	=	Stefan Boltzmann constant ($5.67 \cdot 10^{-8}$ W/m ² K ⁴)
a_p	=	Surface area of particle (m ²)
N_{av}	=	Avogadro's constant
d_p	=	Particle size (used in model)

I. Introduction

METAL particles have been extensively used as additive for energetic compositions owing to their high energy density and reactivity. Aluminum has been the fuel of choice for the such energetic additives although recently other fuels such as titanium and zirconium have also been explored for applications in fire safety, pyrotechnics and flame synthesis.^{1,2} Owing to their boiling points (Ti: 3560 K, Zr: 4650K) being higher than the respective oxide volatilization temperatures, the combustion of Ti and Zr are dominated by surface reactions rather than the metal vapor burning in the gas phase (Glassman's criterion).³ For micron-sized particles, Badiola and Dreizin (Ref. 2) recently measured the combustion temperature of the particles, to be 3343 K for Ti and 3683 K for Zr, which are close to their adiabatic flame temperatures. The burning of these particles were characterized by micro explosions owing to the dissolution and release of nitrogen from the burning surface. With the advent of improved particle generation capabilities at the nanoscale, most recent research in this field has swayed to the examination of nanomaterials owing to their higher reactivity and reduced ignition delay times.⁴

Although there are clear benefits of incorporating metal nanoparticles in highly energetic formulations, there are several complexities such as the nature and the contribution of oxide shell, particle aggregation and sintering which are as yet unresolved. Most significantly the nature of the size dependence on the reaction rate for sub-micron particles are poorly described.^{2,5} The reaction rate for particles have long been correlated to their burn time, which for super micron particles (>30 μm) have been shown to obey the "d²" law, implying a diffusion limited mechanism. As the particle size shrinks, the diffusion length scale reduces, allowing the flame to come very close to the surface of the burning particle, no longer being limited by the diffusion of the reactant species. In this scenario, the surface reactions and their kinetics start dominating, which is exemplified by the shift to a "d¹" law. For particles smaller than 1 μm , the relationship between burn time and particle diameter is currently unclear. The very limited experimental studies indicate a power law with the exponent as 0.3-0.5.^{5,6} Furthermore, nanoparticles seldom remain as single units owing to the weak Van der Waals forces, which lead to particle agglomeration. Such agglomerates pose the problem of rapid sintering prior to the bulk of the reaction, a possibility that has not been explored much in the literature of nanoparticle combustion. A recent work⁷ utilizing molecular dynamics simulation argued that small, aggregated particles do not necessarily remain nano-sized during oxidation due to rapid sintering, with the characteristic reaction time being

comparable to the characteristic sintering time. More recently in-situ dynamic TEM studies have provided experimental proof on the rapid loss of nano structure and concluded that significant morphological changes may occur very early in the reaction process, implying that the bulk of the energy release chemistry occurs in an effectively larger particle.⁸ In this paper we are interested in addressing the nature of the latter lack of clarity for the oxidation of oxide free metal nanoparticles.

II. Experimental Procedure

In this study, nano-sized metal particles of Ti and Zr were generated through laser ablation in an inert environment and were subsequently directed into the post flame region of a laminar diffusion flame for further oxidation studies.

A. Particle Generation and Mobility based size selection

In our experiments, a Q-switched Nd:YAG pulsed laser (Brilliant, Quantel) was operated at 1064 nm, with a pulse energy of 120 mJ at 20 Hz and a pulse width of ~5 ns. The pulsed beam was focused with a fused silica plano-convex lens (150 mm FD) to an energy density of $\sim 10^{10}$ W/cm² to create a local plasma. The target was a 1" diameter, high purity (99.995%) sputter target of the respective metals (Kurt Lesker). The schematic of the assembly is shown in Fig. 1. The metal target was mounted on the rotating shaft of a stepper motor, and the target surface was carefully positioned at the focal point of the lens. The laser spot is about 0.5 mm in diameter at the target surface. In the experiment, argon was flowed (99.995%) across the ablating surface at 1.5 lpm in order to carry the resulting nucleated particles to the DMA. The flow also acted as quenching gas to suppress further particle growth in the laser-induced plume. The laser ablation system was run continuously during the experiments, and did not show any significant variation in the particle size distribution.

For size resolved measurements a DMA (3085, TSI) was modified and mounted upon the laser ablation chamber. The DMA has a cylindrical configuration and consists of two electrodes. The inner electrode is held at a high voltage (0-10 kV) and the outer cylinder is grounded. The electric field created between the inner and outer electrode (Fig. 1) results in a size dependent radially inward electrical mobility for charged particles and is the basis for the size separation.⁹ The metal particles generated by laser ablation are intrinsically charged owing to the high temperature in the laser-induced plasma. The generated particles were subsequently brought to Boltzmann equilibrium by neutralizing the aerosol using a Polonium source of alpha particles. At a fixed voltage, the DMA operates as a band-pass filter for mobility size, and can be employed as a size selection tool. While argon was used in the ablation chamber we found it necessary to use N₂ (99.95%) as the sheath flow (4 lpm), owing to its higher breakdown voltage than argon. The mono-disperse particle flow was kept as 1.5 lpm, which was equivalent to the chamber inlet argon inflow. The DMA used in this work was calibrated with another DMA (3081, TSI) coupled to a condensation particle counter (CPC, 3776, TSI) to obtain the size distribution of particles emanating from the chamber.

B. Flat flame burner and high speed videography

In order to examine the reaction rate of the nanoparticles, they were injected into a high temperature, oxidizing zone which was sustained by the exhaust gases of a flat flame CH₄/O₂/N₂ diffusion flame (Hencken burner). The flame was operated in fuel lean conditions ($\phi = 0.25$) so that there was sufficient oxygen available to oxidize the metal nanoparticles. The stoichiometry of the flame could be varied which helped in adjusting the temperature of the oxidizing zone between 1700K and 2500K.¹ After size selection, the particle-laden flow was injected into a central tube (O.D. 1/16", I.D. 0.022") along the centerline of the cylindrical burner as depicted in Fig. 1.

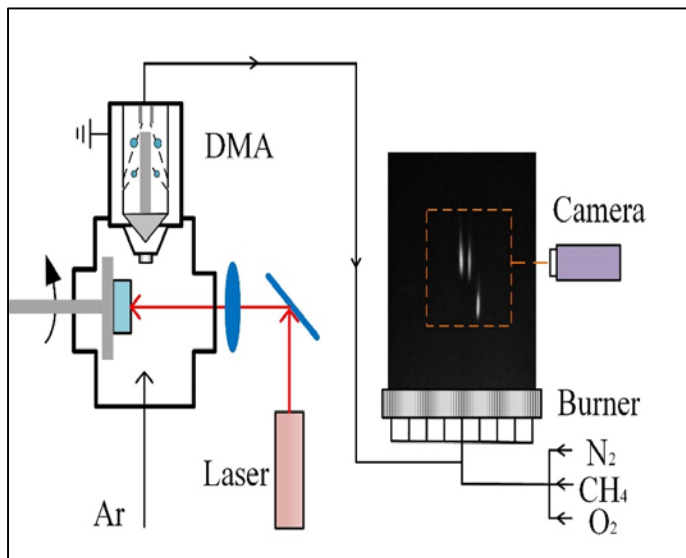


Figure 1. Schematic of particle generation and DMA selection. Particle generated via pulsed laser ablation is mobility size selected using an online DMA and sent to the post flame region of a 1-D laminar diffusion burner.

To evaluate the total burn time, the particle luminosity was tracked with a high-speed camera (Phantom V12.1, Vision Research) with an exposure setting of 5 ms, which is much longer than the particle burn time. Thus the entire combustion event was recorded on a single frame as a streak (Fig. 1), whose length could be used to extract the burn time. The velocity field above the burner was determined by using the camera to track micron-sized seed particles of aluminum. The centerline velocity was measured as 20 ± 2 m/s within the monitored zone for particle burning. At different heights above the burner, the metal particles were sampled by a nanometer aerosol sampler (3089, TSI) and characterized by a Transmission Electron Microscope (JEM 2100, JEOL).

III. Results and Discussion

A. Particle size selection and morphology

The size selection of the generated particles is performed using a DMA, producing a monodisperse aerosol of nanoparticles at each applied voltage. The equation relating particle mobility and the cylindrical DMA parameters are shown in Eq. (1). The particle mobility can also be related to its diameter using Stokes law, as shown in the right half of Eq. 1.

$$Z_P = \frac{Q_{sh}}{2\pi VL} \ln\left(\frac{R_2}{R_1}\right) = \frac{eC}{3\pi\mu d_m} \quad (1)$$

Where Z_P is the particle electrical mobility, Q_{sh} is the DMA sheath flow rate, V is the applied voltage, L, R_1, R_2 are the geometric length, inner and outer diameter of the DMA, e is the charge on the particle (unit charge), C is the Cunningham slip correction factor, μ gas viscosity and d_m is the equivalent spherical particle mobility diameter. This equation can be solved for a diameter vs. voltage dependence which is shown in Fig. 2. A few caveats to take into account during particle generation is that in order to get a highly monodisperse stream the resolution of the DMA needs to be adjusted which is done by tuning the ratio of the sheath flow rate and the aerosol flow rate. Increasing this ratio narrows the range of the particle diameters selected but also reduces the number concentration at the output. Secondly, as laser ablation results in a high temperature plasma, the generated particles have a propensity to accumulate higher charges than unity. This multiple charging can affect the size distribution of the DMA selected aerosol (see Eq. 1) and was corrected by incorporating a radioactive neutralizer (Po source, alpha radiation) which brought the aerosol to a Boltzmann charge distribution.

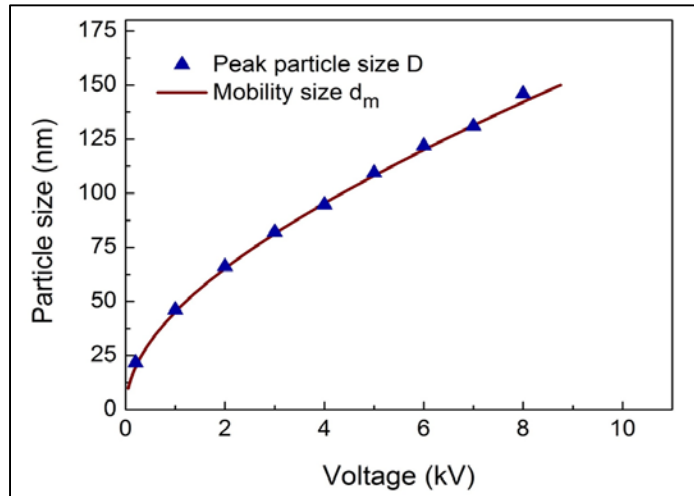


Figure 2. Peak size vs DMA applied voltage. Peak size of the DMA selected particle aerosol as a function of applied voltage.

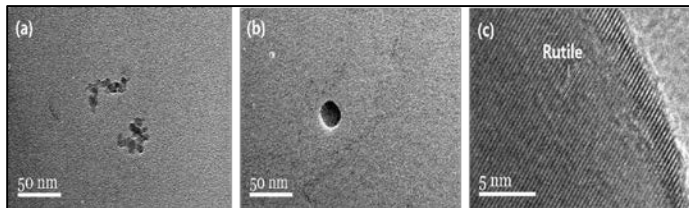


Figure 3. Morphology of Ti particles before and after combustion. (a) Aggregates obtained when DMA selection was set to 21.7 nm peak size, (b) resulting particle morphology post oxidation, and (c) HRTEM image showing the rutile structure of the oxidized particles.

The selected particles were analyzed under a high resolution Transmission electron microscope which revealed that the selected aerosol stream generally consisted of aggregates with a primary particle dimension of 10.3 ± 0.4 nm. Once this particle stream was introduced into the high temperature zone of the burner and subsequently collected, the resulting particle morphology changed from aggregates to spherical as shown in Fig. 3. HRTEM analysis revealed that, for the case of Ti, the oxidized particles post flame was rutile TiO_2 which suggests that complete oxidation did

occur. Similar results were also obtained for Zr case.

B. Combustion characteristics and burn time measurements

As shown in Fig. 1, the particles of both Ti and Zr are observed to exhibit short emission streaks after ignition, which are quite different from those observed for micron-sized particles.² No micro-explosions were observed for the nano-sized particles and the emission streaks were intense and continuous. The major advantage in this study is that the dilute loading of the aerosol enables us to study small agglomerates aiding to tweeze out kinetic effects at the nano scale, as will be shown later.

Burn times were measured for size-selected particles in the range of 20 to 150 nm. For each particle size, 20 emission streaks were tracked and the average burn time was used to plot Fig. 4a (Ti) and Fig. 4b (Zr) as a function of the peak particle size measured after size selection. Under the particles size range considered, the burn times of both metals increase as the particle size increases. We also note that for the size selected burn times, the uncertainty bars are small (2%~9%), indicating that particles of a given size have a very narrow range of burn times. The average burn times for both sets of nanoparticles were in the range of 0.02-0.08 ms with the average burn time of Zr being slightly shorter than Ti, consistent with that found for micron-sized metals.² The burn time measurements were subsequently fit to a power law of the form: $t = aD^b$, where 't' is the measured burn time and D is the DMA selected particle diameter, and the results are shown in Fig. 4.

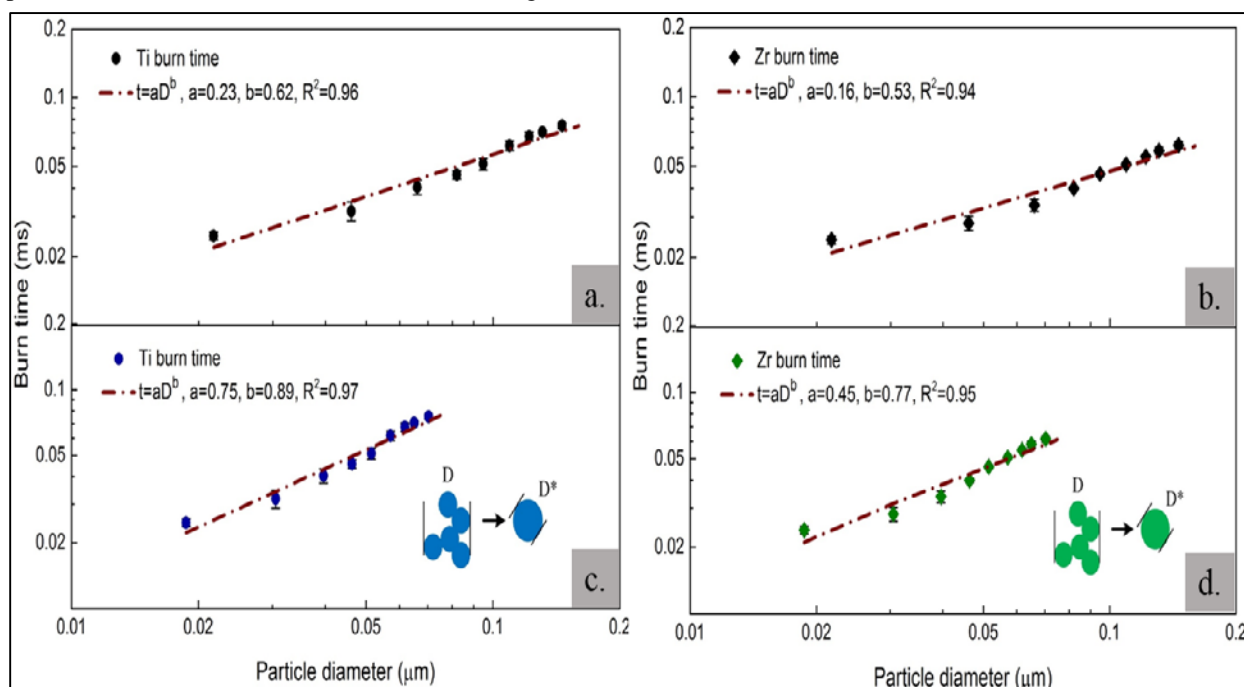


Figure 4. Ti and Zr burn time measurements. Burn time plot of Ti NPs scaled to: (a) DMA peak size, (c) effective sintered size. Burn time plot of Zr NPs scaled to: (b) DMA peak size, (d) effective sintered size.

Our measured exponents are slightly larger than the 0.3-0.5⁵ values observed for Al and show values well below unity, which again cannot be explained by standard theory. The exponent is also larger than what was reported for micro-sized Ti and Zr particles² although in that case the fractional exponent was attributed to the significant micro explosions. As alluded to previously, there is increasing evidence that nanoscale energetics can undergo significant sintering prior to the majority of the heat release. If such sintering is indeed rapid, then using the peak particle diameter in the scaling law would not be an accurate representation. This thinking is inspired by the TEM images presented in Fig. 3 and our recent results on high heating rate TEM studies which observed ultra-fast loss of nanostructure for nanoparticles (on the order of 50 ns).⁸ In order to determine the effect of sintering on the apparent burn time scaling law we have to redefine the particle size assuming fast sintering prior to combustion.

The sintered particle size can be estimated based on the understanding of the evolution of aerosol generated fractal aggregates,¹⁰ which can relate the mobility diameter of a fractal aggregate (d_m) to the number of primary particles present in the aggregate (N) and the primary particle diameter (d_p), as shown in Eq. 2. Once the effective number of primary particles in the aggregate is estimated, the sintered size (D^*) can be calculated by doing a volume conservation, as shown in Eq. 2.

$$d_m = d_p N^{0.46} \quad ; \quad D^* = d_p N^{1/3} \quad (2)$$

Sintering affects larger sized aggregates more, thus the rescaling of the size axis is most pronounced at the large size end. With this renormalization, we replot our burn times in Figs. 4c and 4d, which we again fit using the same power law, $t = aD^b$. As can be seen, the new exponents are larger than the ones that were previously calculated and are now slightly smaller than unity, which is expected from a heterogeneous combustion mechanism.

Owing to the extremely short streaks of the nanoparticle aggregates, we can conservatively assume that the burning particle would more or less experience an isothermal environment during combustion. Based on the temperature profiles of the oxidation zone,¹ the temperature differential over the length of an average streak was estimated to be ~20 K. This enables us to use isoconversion techniques developed for calorimetric analysis to derive effective Arrhenius parameters for the oxidation of these nanoparticles. For these studies we limited the measurement to only one particle size (peak size: 145.9 nm) and studied the effect of ambient temperature by analyzing the streaks observed at various flame conditions. Burn times as expected decrease with increasing temperature. We obtain a pre-exponential factor of $7.5E5 \text{ s}^{-1}$ and an activation energy of 56 kJ/mol for Ti; and $3.4E5 \text{ s}^{-1}$ and 43 kJ/mol, for Zr, which are within the same order of magnitude as reported for other metals in the nanoscale size regime.⁶

C. Combustion Modelling

The observed spatially resolved emission intensity is a direct window into the burning process, which enables us to tweeze out the underlying reaction mechanism. The burning streak from a 40 nm size selected Ti particle is shown in Fig. 5. This particular streak has a burn time of $40 \mu\text{s}$ as demarcated by the dashed vertical line thresholded at 10% of peak intensity. Since the intensity of the streak can be correlated to the temperature ($I \sim T^4$), the streak profile, normalized with peak intensity, can be used as a representative of the temperature.

Since the TEM images reveal final product sizes being larger than the primary particles of the initial agglomerates, a reaction mechanism where the reactant species diffuse through the ash layer seems to be the case. Several reaction models of the form $da/dt = k(T) * f(a)$ were evaluated, where, $k(T)$ is the rate constant (inverse of burn time (τ , fixed) and $f(a)$ is the reaction model as a function of the conversion factor (α).¹¹ The three main reaction models used were (X_{Ti} represents the volume fraction of unreacted core):

*Shrinking core-Kinetic mode:*¹²

$$\frac{dX_{Ti}}{dt} = \frac{(-3) * X_{Ti}^{2/3}}{\tau} \quad (3)$$

Shrinking core-Diffusion through Ash layer:

$$\frac{dX_{Ti}}{dt} = \frac{1}{2\tau(1-X_{Ti}^{-1/3})} \quad (4)$$

*Avrami-Erofeev Nucleation model (AE 4):*¹¹

$$\frac{dX_{Ti}}{dt} = \frac{(-4) * X_{Ti} * (-\log(X_{Ti}))^{0.75}}{\tau} \quad (5)$$

If the diffusion of the reactant species is fast through the ash layer, then a kinetic controlled reaction of the kind (3) would be an accurate representation. If the kinetics are fast and diffusion is rate limiting, then Eq. (4) would provide a better fit to the emission profile. Some recent work² on Titanium combustion suggested the dissolution of oxygen into the unreacted core as a reaction mechanism. This dissolved oxygen could react with the unreacted core forming nuclei of the oxide within the particle, justifying the use of Eq. 5. In addition to the aforementioned, several power law models, Prout-Tompkins model, Ginstling-Brounstein diffusion models were also evaluated.¹¹

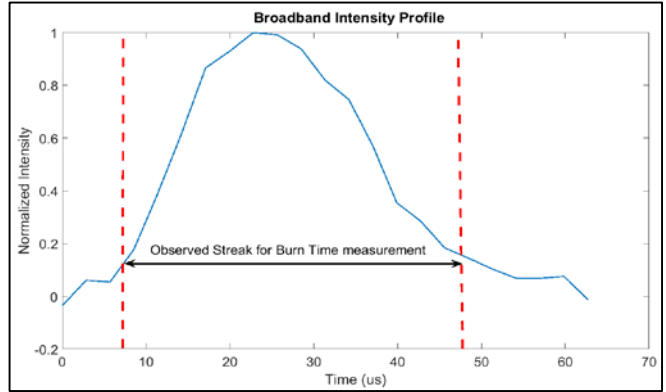


Figure 5. Broadband Emission Profile of a 40 nm Ti Particle.

The heat transfer from the particle was modelled as the sum of radiation, conduction and evaporation terms. Evaporative heat transfer was derived from collision theory based on detailed balancing.¹³ Conduction heat transfer was derived from the collision of gas molecules with the particle. Some recent results¹⁴ regarding conduction heat transfer highlighted the poor efficiency of heat transfer via conduction. The authors claimed that the gas particle collisions at the nanoscale were not 100% efficient (the ratio termed as Energy Accommodation Coefficient, EAC) and suggested that the EAC values were as low as 0.005 instead of a nominal value of 1. Due to the lack of widespread confirmation, we kept the EAC as a free parameter in our fitting procedure. The net heat loss was formulated as:

$$Q_{loss} = \frac{\left\{ \alpha \pi \left[\frac{d_p}{2} \right]^2 \frac{P_g}{2} \left[\frac{8KT_g}{\pi m_g} \right]^{0.5} \frac{(\gamma+1)(T-T_g)}{(\gamma-1)T_g} \right\}}{\text{Conduction term}} + \frac{\left\{ \epsilon_{avg} \sigma \pi d_p^2 (T^4 - T_g^4) \right\}}{\text{Radiation term}} + \frac{\left\{ \frac{1 * P_S a_p}{\sqrt{2} \pi K T_p} \frac{\Delta H_{volalization}}{N_{av}} \right\}}{\text{Evaporation term}} \quad (6)$$

Where, α is the EAC, d_p is particle diameter, P_g : gas pressure (1 atm), m_g : air molecular weight ($4.8 \cdot 10^{-26}$ Kg), T : particle temperature [K], T_g : gas temperature (1750 K), γ : adiabatic expansion factor (=1.3 at 1500 K), a_p : surface area of particle (m^2), ϵ_{avg} : molar average emissivity, N_{av} : Avogadro's constant, K : Boltzmann Constant ($1.38 \cdot 10^{-23}$ m² Kg s⁻² K⁻¹). The set of equations were solved numerically to yield temporal plots of the emission intensity from the particle.

The model simulations and the experimental emission profile of the 40 nm particle in Fig. 5 is shown in Fig. 6a. As shown in the figure, it can be seen that using a low value of EAC (0.005) does not provide good fits for any of the aforementioned models. Hence we treated EAC as a free parameter to get the best fit and the result is shown in Fig.

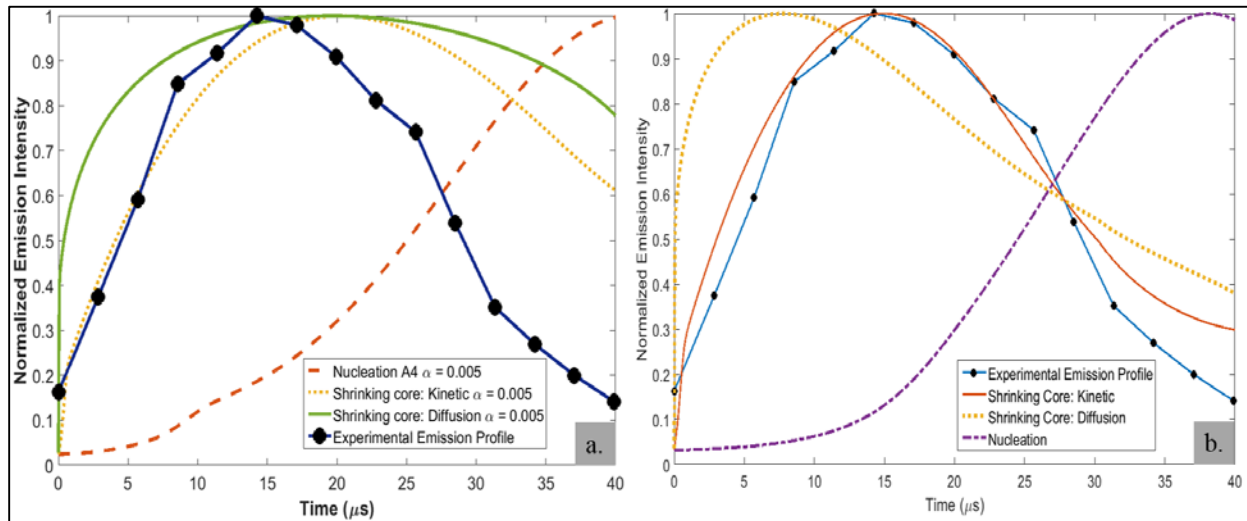


Figure 6. Model simulations for 40 nm particle. Emission plots with: (a) EAC = 0.005, (b) EAC = 0.3.

6b. As shown in the figure, the kinetic controlled shrinking core model with EAC of 0.3 seems to provide the best fit for the experimental emission profile, strengthening the previous argument that the oxidation of nanoscale Ti and Zr is limited by the kinetics of the heterogeneous mechanism. Similar profiles were also obtained for larger and smaller particle sizes as well as for Zirconium.

D. Strategies to improve the combustion performance of nanoenergetics⁴

The previous sections highlight the effect of rapid sintering on the combustion of metal nanoparticles and suggests that the oxidation kinetics at the nanoscale is primarily a kinetic limited process. The rapid loss of nanostructure due to sintering with nearby particles is of course a detriment leading to the low power dependence to the oxidation scaling law. We have explored several strategies to increase the rapidity of reaction relative to sintering. One approach we have found to be promising is to assemble nanoparticles into microscale mesoparticles incorporating a gas generator, as shown in Fig. 7. The gas generator, upon heating, decomposes at a lower temperature than the sintering temperature resulting in the disintegration of the composite, thereby reducing the average distances between the individual particles and reducing their propensity to sinter. This strategy was successfully tested in our lab using nitrocellulose as the energetic gas generator/binder.^{4,15} Aluminum nanoparticles and nitrocellulose were packaged into micron sized composites via electrospray. These composites were subsequently injected into the oxidizing zone of the burner

assembly shown in Fig. 1. The low decomposition temperature of nitrocellulose (~170 C) results in gas generation within the composites at a temperature lower than the metal particle ignition thereby shattering the composite before bulk of the energy release. A direct comparison of the burn times with that of the parent nanoparticles in its native aggregated state revealed an order of magnitude reduction in burn times when using this strategy to mitigate sintering. Such strategies, could be considered for incorporated into future compositions of nanomaterials so as to maximize their potential of enhanced reaction rate and lower ignition delay times.

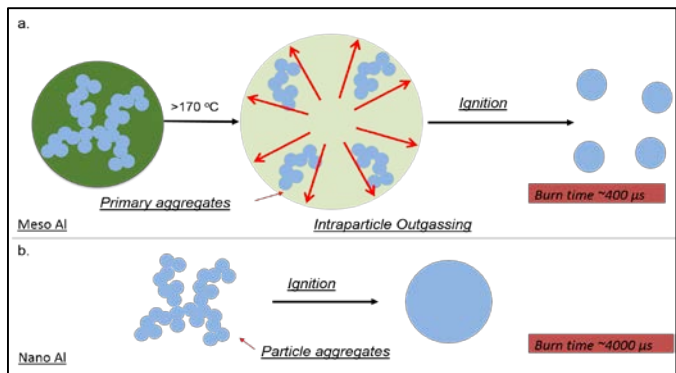


Figure 7. Incorporation of Nitrocellulose to mitigate sintering. Burning of (a) nanoAl mesoparticles. (b) nanoAl aggregates in native state.

IV. Conclusion

An atmospheric pressure laser ablation system coupled to a differential mobility analyzer (DMA) was used to produce size-resolved metal particles of titanium and zirconium in the range of 20-150 nm. The ignition and combustion characteristics of the metal particles were investigated in the post flame region of a flat flame burner, with the oxidizing zone temperature ranging from 1700 K to 2500 K. The Ti and Zr nanoparticles exhibited clear short emission streaks after ignition, which are quite different from those observed for micro-sized particles. From the TEM images it was deduced that the particles coalesce during combustion and transform from aggregates to sintered spherical particles. After accounting for the effects of sintering we find the burn time obeys a near d^1 power law. Additionally, the emission intensity profile from individual particles was used to benchmark several kinetic models. It was found that the best fit to the experimental data was obtained by using a shrinking core model that was limited by the surface oxidation kinetics. Furthermore, a successful strategy of packaging nanomaterials into smart composite structure has been suggested which could potentially help in enhancing the potential benefits of nanoenergetics.

Acknowledgments

This work was supported by the Army Research Office, and an AFOSR-MURI, and was performed at the University of Maryland. We also thank the support from the University of Maryland Nano center. YCZ also acknowledges the National Natural Science Fund of China (No. 51176094) for their support.

References

- ¹Zong, Y. C., Jacob, R. J., Li, S. and Zachariah, M. R., "Size Resolved High Temperature Oxidation Kinetics of Nano-Sized Titanium and Zirconium Particles," *Journal of Physical Chemistry A*, Vol. 119, No. 24, 2015, pp. 6171, 6178.
- ²Badiola, C., Dreizin, E. L., "Combustion of Micron-Sized Particles of Titanium and Zirconium," *Proceedings of the Combustion Institute*, Vol. 34, No. 2, 2013, pp. 2237–2243.
- ³Yetter, R. A., Risha, G. A., Son, S. F., "Metal Particle Combustion and Nanotechnology," *Proceedings of the Combustion Institute*, Vol. 32, No. 2, 2009, pp. 1819–1838.
- ⁴Jacob, R. J., Wei, B., Zachariah M. R., "Quantifying the enhanced combustion characteristics of electrospray assembled aluminum mesoparticles," *Combustion and Flame*, 2015, (In Press).
- ⁵Huang, Y., Risha, G. A., Yang, V., Yetter, R. A., "Combustion of bimodal nano/micron-sized aluminum particle dust in air," *Proceedings of the Combustion Institute*, Vol. 31, No. 2, 2007, pp. 2001–2009.
- ⁶Young, G., Sullivan, K., Zachariah, M. R., Yu, K., "Combustion Characteristics of Boron Nanoparticles," *Combustion and Flame*, Vol. 156, No. 2, 2009, pp. 322–333.
- ⁷Chakraborty, P., Zachariah, M. R., "Do Nanoenergetic Particles Remain Nano-Sized during Combustion?," *Combustion and Flame*, 161, Vol. 161, No. 5, 2014, pp. 1408–1416.
- ⁸Egan, G. C., Sullivan, K. T., LaGrange, T., Reed, B. W., Zachariah, M. R., "In Situ Imaging of Ultra-Fast Loss of Nanostructure in Nanoparticle Aggregates," *Journal of Applied Physics*, Vol. 115, No. 8, 2014, pp. 084903.
- ⁹Guha, S., Li, M., Tarlov, M. J., Zachariah, M. R., "Electrospray-Differential Mobility Analysis of Bionanoparticles," *Trends in Biotechnology*, Vol 30, No. 5, 2012, pp. 291–300.

¹⁰Sorensen, C. M., "The Mobility of Fractal Aggregates: A Review," *Aerosol Science and Technology*, Vol. 45, No. 7, 2011, pp. 765–779.

¹¹Khawam, A., Flanagan, D. R., "Solid-State Kinetic Models: Basics and Mathematical Fundamentals," *Journal of Physical Chemistry B*, Vol. 110, No. 35, 2006, pp. 17315–17328.

¹²Levenspiel, O., "Chemical Reaction Engineering," 3rd ed., *John Wiley & Sons: New York*, 1999.

¹³Mukherjee, D., Sonwane, C. G., Zachariah, M. R., "Kinetic Monte Carlo Simulation of the Effect of Coalescence Energy Release on the Size and Shape Evolution of Nanoparticles Grown as an Aerosol," *Journal of Chemical Physics*, Vol. 119, No. 6, 2003, 3391-3404.

¹⁴Allen, D., Krier, H., Glumac, N., "Heat Transfer Effects in Nano-Aluminum Combustion at High Temperatures," *Combustion and Flame*, Vol. 161, No. 1, 2014, 295–302.

¹⁵Wang, H., Jian, G., Egan, G. C., Zachariah, M. R., "Assembly and reactive properties of Al/CuO based nanothermite microparticles," *Combustion and Flame*, Vol. 161, No. 8, 2014, 2203–2208.